J Solid State Electrochem (2000) 4: 314–324

ORIGINAL PAPER

Uwe Schröder · Keith B. Oldham · Jan C. Myland
Peter J. Mahon · Fritz Scholz

Modelling of solid state voltammetry of immobilized microcrystals assuming an initiation of the electrochemical reaction at a three-phase junction

Received: 24 November 1999 / Accepted: 22 February 2000

Abstract The electrochemical reduction of a solid compound characterized by mixed ionic/electronic conductivity, immobilized on an electrode surface and in contact with an electrolyte solution, has been studied theoretically. The uptake or expulsion of electrons and electrolyte cation

$$Ox_{solid} + e^-_{electrode} + C^+_{solution} \rightleftharpoons RedC_{solid}$$

is coupled to maintain electroneutrality and is assumed to obey Fick's law of diffusion. Starting with the fully oxidized species, the simultaneous uptake of cations and electrons will be possible at the three-phase junction only, where electrode, solid and electrolyte solution meet. From this point, electrons and cations diffuse perpendicularly into the crystal lattice. The reaction zone grows owing to the formation of the electronically and ionically conducting reduced product. Two- and three-dimensional models have been utilized to simulate the diffusion and the current flow in response to an applied potential step. The resulting chronoamperometric curves have been analyzed with the help of fitting procedures. Under certain conditions, a transition of the three-phase reaction to a pure two-phase reaction occurs. This transition to a two-phase condition is the reason that a number of equations for the exhaustive conversion are similar to those known for planar diffusion, for example. To illustrate this, and for a better understanding of the phenomena, concentration profiles are presented for different degrees of the reaction and for varied simulation conditions. It is demonstrated how geometrical properties like crystal shape (cuboid with $x \neq y \neq z$) and crystal size as well as physical properties, e.g. the diffusion coefficients, govern the electrochemical behavior of mixed ionic/electronic conductors and form the basis of the current-time functions. The numerical simulation of a two-dimensional semi-infinite model of the reaction at the three-phase junction gives results comparable to an algebraical approach. The finite-difference method turned out to be suitable to solve the problems arising from the three-dimensional and finite diffusion conditions and from different crystal shapes.

Key words Voltammetry · Microparticles · Modelling · Three phase junction

Presented at the international conference "Modern Electroanalytical Methods", 19th to 23rd September, 1999, in Seč, Czech Republic

U. Schröder[1] · F. Scholz (✉)
Ernst-Moritz-Arndt-Universität,
Institut für Chemie und Biochemie,
Soldmannstrasse 16, 17487 Greifswald, Germany

K.B. Oldham · J.C. Myland · P.J. Mahon[2]
Electrochemical Laboratory, Trent University,
Peterborough, Ontario, K9J 7B8, Canada

Present addresses:
[1]Physical and Theoretical Chemistry Laboratory,
Oxford University, South Parks Road,
Oxford OX1 3QZ, UK
[2]cap-XX Pty. Ltd., North Ryde 2113, NSW, Australia

List of symbols

B crystal width (cm) · c concentration (mol cm^{-3}) · Δx (Δx_0) length of the bulk (surface) boxes (cm) · Δy (Δy_0) width of the bulk (surface) boxes (cm) · Δz (Δz_0) height of the bulk (surface) boxes (cm) · D_{C^+} diffusion coefficient of cations inside the crystal (cm^2 s^{-1}) · D_{e^-} diffusion coefficient of electrons inside the crystal (cm^2 s^{-1}) · E applied electrode potential (V) · E_f formal potential (V) · E^0 standard potential (V) · $f_{\{\}}$ activity coefficient of a species within the solid phase · f_{shape} symmetry factor representing the influence of a overlapping cation diffusion in the three-dimensional model · F Faraday constant (C mol^{-1}) · H crystal height (cm) · L crystal length (cm) · k,m,l box indices for the x, y and z directions · $I(t)$ net current (A) · $I_s(t)$ surface current (A) · $I_b(t)$ bulk current (A) · j dimensionless integer · j_{C^+}, j_{e^-} flux of cations or flux of electrons (mol cm^{-2} s^{-1}) · N amount (mol) · t time (s) · ϕ dimen-

sionless potential · β dimensionless diffusion coefficient · v see Eq. 19 · V_m molar volume ($cm^3\ mol^{-1}$) · Y length of the three-phase junction.

Introduction

The voltammetry of microcrystals enables the analysis of a wide range of compounds [2]. The technique is based upon immobilization of trace amounts of a solid sample on the surface of an electrode. It can provide a means to study the electrochemical behavior of solid compounds which is important, for example, for battery or sensor development. One group of materials of special interest are compounds which exhibit mixed ionic/electronic conductivity. This means that the electrochemical redox reaction is accompanied by an insertion and expulsion of ions from or into the adjacent solution. In order to maintain electroneutrality the transport of electrons and ions has to proceed at the same rate. It has been shown that both the transport of the ions and the electrons obeys Fick's laws of diffusion [3]. The transport of the electrons in the lattice (electron hopping) can be understood in terms of an exchange reaction:

Red-Ox-Ox ⇒ Ox-Red-Ox

The consequences of such a coupled diffusion mechanism on the voltammetric behavior are not straightforward and require thorough investigation. Initial theoretical approaches describing the reaction at the three-phase junction with the help of a two-dimensional semi-infinite model were carried out by Lovric and Scholz [1]. A different approach has been presented by Oldham [4]. It is based on the diffusion through the "bottleneck" of the three-phase junction. Oldham could demonstrate a sustained reaction with ion supply through the three-phase junction to be possible within a voltammetric time scale.

The emphasis in this paper is the simulation of a single-crystal potential-step experiment to answer the following questions. How does the shape and the size influence the electrochemical conversion of an immobilized microcrystal? Is it possible to derive geometric parameters or the individual diffusion coefficients from a chronoamperometric curve? Can geometric parameters be determined and can two-dimensional models give information comparable to a three-dimensional approach?

Theory

Consider a solid state electrochemical redox reaction, which requires an insertion of cations to maintain electroneutrality:

$$Ox_{solid} + e^-_{electrode} + C^+_{solution} \rightleftharpoons RedC_{solid} \quad (1)$$

At the three-phase boundary, thermodynamic equilibrium is established according to:

$$\frac{a_{\{RedC\}}}{a_{\{Ox\}}} = \exp(\varphi) \quad \text{with} \quad \varphi = \frac{F}{RT}(E_f - E) \quad (2)$$

where E is the potential; E_f is the formal potential of the reaction:

$$E_f = E^0 + \frac{RT}{F}\ln\frac{f_{\{ox\}}}{f_{\{red\}}} - \frac{RT}{F}\ln K + \frac{RT}{F}\ln a_{C^+_{solution}} \quad (3)$$

with

$$K = \frac{a_{\{Red^-\}}a_{C^+_{solution}}}{a_{\{RedC\}}} = \frac{f_{\{Red^-\}}c_{\{Red^-\}}a_{C^+_{solution}}}{f_{\{RedC\}}c_{\{RedC\}}}$$

where E^0 is the standard potential of the reaction and K is the equilibrium constant of the cation transfer between the crystal and the electrolyte solution.

It is assumed that the molar volume V_m ($cm^3\ mol^{-1}$) of the redox centers remains unchanged during the redox process. Thus, the formal concentrations of Ox and RedC are related to their activities as $c_{\{Ox\}} = a_{\{Ox\}}/V_m$, $c_{\{RedC\}} = a_{\{RedC\}}/V_m$ with $a_{\{RedC\}} + a_{\{Ox\}} = 1$. It is also assumed that owing to an excess of electrolyte the cation concentration in the solution remains unaffected by the redox process inside the solid. Any kinetic limitations of the reaction are ignored.

Grid properties

Assume a coordinate system (x,y,z), as in Fig. 1, in which a crystal occupies $0 \le x < \infty$, $-\infty < y < \infty$, $0 \le z < \infty$. The ($x > 0$,y,0) plane is the electrode|crystal interface, (0,y,z) is the electrolyte|particle interface and the line (0,y,0) represents the three-phase junction, where electrolyte, electrode and crystal meet. The basic property of the two-dimensional model is that there is no dependence on the y-coordinate at any time during the simulated experiment. The modelling can thereby be reduced to the x,z-matrix demonstrated in Fig. 2. The matrix consists of discrete boxes with the indices (k,m) and a box area of $\Delta x_k \Delta z_m$ (Fig. 2). To obtain a box volume, the box area is multiplied with a normalized length of the three-phase junction y.

In order to take the different physical properties of the crystal's surface layers (crystal|electrode and

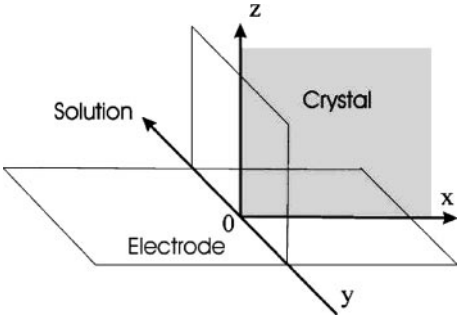

Fig. 1 Coordinate system showing a part of the electrode surface (x,y,0) with $-\infty < x,y < \infty$ and a part of the particle|solution interface (x,0,z) with $0 < x,z < \infty$

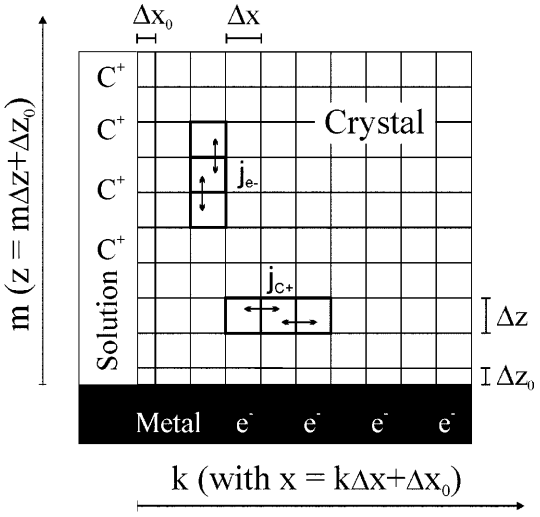

Fig. 2 Two-dimensional matrix of discrete boxes with $\Delta x\Delta z$ being the size of the bulk boxes, $\Delta x_0\Delta z$ and $\Delta x\Delta z_0$ being the size of the surface boxes and $\Delta x_0\Delta z_0$ representing the three-phase junction

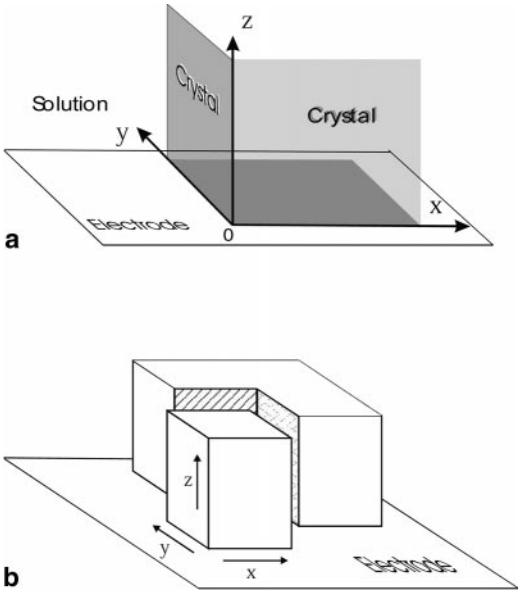

Fig. 3 Coordinate system showing a part of the electrode surface $(x,y,0)$ with $-\infty < x,y < \infty$ and a part of the crystal|solution interface $(x,0,z)$ with $0 < x,z < \infty$ and $(0,y,z)$ with $0 < y,z < \infty$. The electrode|crystal interface occupies $(x,y,0)$ with $0 < x,y < \infty$. **b** Schematic drawing of a cuboid microcrystal. The calculations have been restricted to one quarter only

crystal|electrolyte interface) into consideration, we distinguish between surface boxes ($k = 0$ for the crystal|solution interface, $m = 0$ for the crystal|electrode interface) and bulk boxes (k and $m > 0$). A problem is the definition of the "surface". Does it contain a real volume (and therefore a volume concentration c) or should one define it as a flat plane with a surface concentration Γ? For the following calculations it has been assumed that the "surface" has a certain thickness, which is considerably smaller in its magnitude than the size of the bulk boxes.

Although finite difference methods utilizing expanding grid algorithms (e.g. DuFord/Frankel) are much faster with respect to the computing speed [5], it was decided to work with a uniform grid because it is easier to handle when additional conditions (finite grid size) are introduced. The size of the applied grid (number of boxes) was always a compromise between poor accuracy in the case of a small number of boxes, on the one hand, and a dramatic decrease of computational speed with a growing number of boxes, on the other hand. This fact is particularly distinctive in the case of three-dimensional grids. Depending on the simulation parameters, arrays with a size up to 250×250 boxes were used for the two-dimensional, semi-infinite model and $100 \times 100 \times 100$ boxes for the three-dimensional model.

Semi-infinite conditions have been simulated, working with the condition that the simulation was aborted when the product concentration inside the edge boxes (marked with the subscript "max" (see Eqs. 10a–f) exceeded a value of about 10^{-6} mol/cm^3. This concentration is an arbitrary value derived from simulated chronoamperograms in combination with the accompanying concentration profiles. In the model it represents the reaction limit where semi-infinite diffusion conditions are found.

The finite diffusion space calculations are based upon the following considerations:

1. The values of the diffusion coefficients, the grid size and the time scale of the simulated experiment enable a complete conversion to product (the abort condition of the semi-infinite model is disabled).
2. The symmetry of the particle shape allows a smaller simulation volume by cutting the two-dimensional grid into two edges and the three-dimensional matrix into four parts (Fig. 3) because the concentration on both sides of the midplane between these parts is always equal and therefore no flux occurs across that plane.

Derivation of the diffusion equations

In the following paragraphs, the algorithm of the modelling will be described in terms of the two-dimensional grid. The three-dimensional grid has been derived analogously, with the extension of the additional flux of cations in the y-direction.

The main assumption of the model is the condition that the cations enter the lattice only through the $(0,y,z)$ interface (see Fig. 1), starting in the vicinity of the three-phase junction. Only there is charge compensation possible. Any cation insertion through the (x,y,z_{max}) crystal|solution interface, which represents the top boundary of a finite crystal, would charge the surface layer like a condenser, compensation not being possible since electrons can enter the crystal only from the opposite $(x,y,0)$ interface.

Because of the localized extent of the electric field, any migration will obey laws similar to those of

diffusion; migration has therefore been lumped in with diffusion in our treatment.

We assume that:

1. The concentrations of the oxidized and reduced centers at the three-phase junction are thermodynamically equilibrated and therefore governed by the Nernst equation [6].
2. The flux of the electrons proceeds in the z-direction only (Fig. 2).
3. The flux of the cations proceeds only in the x-direction (perpendicular to the electron flow).

The total flux of electrons and cations is a function of the concentration gradients between each box (k,m) and its two neighbor boxes (denoted by a subscript "n"). It follows Fick's first law of diffusion:

$$j_{C^+} \equiv \frac{1}{Y\Delta z}\frac{\Delta N}{\Delta t} = -D_{C^+}\sum_2 \frac{\Delta C}{\left(\frac{\Delta x}{2}+\frac{\Delta x_n}{2}\right)} \tag{4a}$$

$$j_{e^-} \equiv \frac{1}{Y\Delta x}\frac{\Delta N}{\Delta t} = -D_{e^-}\sum_2 \frac{\Delta C}{\left(\frac{\Delta z}{2}+\frac{\Delta z_n}{2}\right)} \tag{4b}$$

where ΔC represents the difference in concentration between two adjacent boxes and ΔN represents the change of the amount (moles) of cations or electrons, with Y representing the length of the infinite three-phase junction.

The c symbol in the following equations represents the concentration of the reduced species, c_{RedC}, which is equivalent to the concentration of cations and electrons. Because $\Delta N = \Delta c Y \Delta x \Delta z$ with $\Delta c = c^{t+\Delta t}_{(k,m)} - c^{t}_{(k,m)}$:

$$\frac{\Delta c}{\Delta t} = -D_{C^+}\sum_2 \frac{\Delta C}{\Delta x\left(\frac{\Delta x}{2}+\frac{\Delta x_n}{2}\right)} \tag{5}$$

Concentration changes of cations with time:

$$\begin{aligned} c^{new}_{(k,m)} - c_{(k,m)} &= D_{C^+}\Delta t\left(\frac{(c_{(k+1,m)}-c_{(k,m)})}{\Delta x_{(k,m)}\left(\frac{\Delta x_{(k,m)}}{2}+\frac{\Delta x_{(k+1,m)}}{2}\right)}\right. \\ &\left. + \frac{(c_{(k-1,m)}-c_{(k,m)})}{\Delta x_{(k,m)}\left(\frac{\Delta x_{(k,m)}}{2}+\frac{\Delta x_{(k-1,m)}}{2}\right)}\right) \end{aligned} \tag{6a}$$

Concentration changes of electrons with time:

$$\begin{aligned} c^{new}_{(k,m)} - c_{(k,m)} &= D_{e^-}\Delta t\left(\frac{(c_{(k,m+1)}-c_{(k,m)})}{\Delta z_{(k,m)}\left(\frac{\Delta z_{(k,m)}}{2}+\frac{\Delta z_{(k,m+1)}}{2}\right)}\right. \\ &\left. + \frac{(c_{(k,m-1)}-c_{(k,m)})}{\Delta z_{(k,m)}\left(\frac{\Delta z_{(k,m)}}{2}+\frac{\Delta z_{(k,m-1)}}{2}\right)}\right) \end{aligned} \tag{6b}$$

In order to simplify the computation, dimensionless diffusion coefficients (β) are introduced. Owing to the assumptions for the surface layer there are two different coefficients to be calculated for the electron and cation diffusion, respectively.

We define:

$$m = 1 \quad \beta^0_{e^-} = \frac{D_{e^-}\Delta t}{\Delta z\left(\frac{\Delta z_0}{2}+\frac{\Delta z}{2}\right)} \tag{7a}$$

$$m > 1 \quad \beta_{e^-} = \frac{D_{e^-}\Delta t}{\Delta z^2} \tag{7b}$$

for the electrons. Similarly, for the cations, we use the definitions:

$$k = 1 \quad \beta^0_{C^+} = \frac{D_{C^+}\Delta t}{\Delta x\left(\frac{\Delta x_0}{2}+\frac{\Delta x}{2}\right)} \tag{7c}$$

$$k > 1 \quad \beta_{C^+} = \frac{D_{C^+}\Delta t}{\Delta x^2} \tag{7d}$$

From Eqs. 6 and 7 it follows that:

$$\begin{aligned} c^{new}_{(k,m)} &= (1-\beta_{C^+_{k-1}}-\beta_{C^+_{k+1}})c_{(k,m)} \\ &\quad + \beta_{C^+_{k-1}}c_{(k-1,m)} + \beta_{C^+_{k+1}}c_{(k+1,m)} \end{aligned} \tag{8a}$$

for the cation diffusion, and:

$$\begin{aligned} c^{new}_{(k,m)} &= (1-\beta_{e^-_{m-1}}-\beta_{e^-_{m+1}})c_{(k,m)} \\ &\quad + \beta_{e^-_{m-1}}c_{(k,m-1)} + \beta_{e^-_{m+1}}c_{(k,m+1)} \end{aligned} \tag{8b}$$

for the diffusion of electrons.

In a more sophisticated theory it will be necessary to take into account the Wagner factor for ions and electrons [7] and to use common and direction-dependent diffusion coefficients D_X, D_Y, D_Z instead of the individual diffusion coefficients D_{C^+} and D_{e^-}.

Mathematical algorithm for the simulation of a potential-step experiment

0. For $t = 0$, the crystal's composition is determined by a thermodynamic equilibrium determined by the applied electrode potential E_{t_0}:

$$c_{(k,1)} = \frac{1}{V_m}\left\{\frac{1}{1+\exp(-\varphi_0)}\right\} \tag{9a}$$

with $\varphi_0 = F(E_{t_0} - E_f)/RT$.

1. For $t > 0$, the concentration at the three-phase junction is a function of the applied potential E:

$$c_{(0,0)} = \frac{1}{V_m}\left\{\frac{1}{1+\exp(-\varphi_t)}\right\} \tag{9b}$$

with $\varphi_t = nF(E - E_f)/RT$.

For the simulation of a chronoamperometric experiment the potential E is held constant. In order to model a potential sweep experiment, the value is shifted according to the sweep rate and the time increment.

2. First, the diffusion of cations along the (k,y,0) plane (the crystal|electrode interface) is calculated. The

concentration of converted material along this interface layer is determined only by the diffusion of the cations from the three-phase junction. Electroneutrality is always ensured, as there is a sufficiency of electrons along the electrode surface.

$$\text{For } k = 1: \quad c^{\text{new}}_{(1,0)} = c_{(1,0)}(1 - \beta^0_{C^+} - \beta_{C^+}) + \beta^0_{C^+} c_{(0,0)} + \beta_{C^+} c_{(2,0)} \tag{10a}$$

$$\text{For } k = 2 \text{ to } k_{\max^{-1}}: \; c^{\text{new}}_{(k,0)} = c_{(k,0)}(1 - 2\beta_{C^+}) + \beta_{C^+}(c_{(k-1,0)} + c_{(k+1,0)}) \tag{10b}$$

$$\text{For } k = k_{\max}: \; c^{\text{new}}_{(k_{\max},0)} = c_{(k_{\max},0)}(1 - \beta_{C^+}) + \beta_{C^+} c_{(k_{\max}-1,0)} \tag{10c}$$

3. Based on the concentration of cations in the $c_{(k,0)}$ row, the electron diffusion into the bulk is calculated:

$$\text{For } k = 0 \text{ to } k_{\max} \text{ and } m = 1:$$
$$c^{\text{new}}_{(k,1)} = c_{(k,1)}(1 - \beta^0_{e^-} - \beta_{e^-}) + \beta^0_{e^-} c_{(k,0)} + \beta_{e^-} c_{(k,2)} \tag{10d}$$

$$\text{For } k = 0 \text{ to } k_{\max} \text{ and } m = 2 \text{ to } m_{\max^{-1}}:$$
$$c^{\text{new}}_{(k,m)} = c_{(k,m)}(1 - 2\beta_{e^-}) + \beta_{e^-}(c_{(k,m-1)} + c_{(k,m+1)}) \tag{10e}$$

$$\text{For } k = 0 \text{ to } k_{\max} \text{ and } m = m_{\max}$$
$$c^{\text{new}}_{(k,m_{\max})} = c_{(k,m_{\max})}(1 - \beta_{e^-}) + \beta_{e^-} c_{(k,m_{\max}-1)} \tag{10f}$$

4. The current is calculated from the concentration change in each box during the time increment Δt:

$$I = F \sum_{k,1} \left[(c^{\text{new}}_{(k,m)} - c_{(k,m)}) \Delta x_k \Delta z_m Y \right] / \Delta t \tag{11}$$

5. The box concentrations are updated and time stepped.

$$\text{For } k = 0 \text{ to } k_{\max}, \text{ for } m = 0 \text{ to } m_{\max}$$
$$c_{(k,m)} = c^{\text{new}}_{(k,m)}$$
$$t \Rightarrow t + \Delta t$$
Return to 1.

Results and discussion

All equations in the following sections are the result of thorough curve fitting procedures based upon specially designed simulation conditions. For that purpose, one or more parameters (geometry, size, diffusion coefficients) were varied and the potential step experiment was simulated. The obtained chronoamperograms have been analyzed using different fitting methods with the aim to find dependencies of the results on the applied model parameters. For semi-infinite conditions the curve analysis has been performed with the help of $i\sqrt{t}$ vs. $\sqrt{t}$ plots. Current/time data describing an exhaustive conversion have been interpreted with exponential decay curve fitting procedures. Additional information could be gained from the concentration profiles, which have been used to visualize the course of the reaction.

Semi-infinite diffusion space

The accuracy of the derived equations was verified with the following procedure:

1. Using the appropriate equation, different sets of current/time values were simulated using varied conditions (crystal size, diffusion coefficients).
2. For the same conditions, the data were calculated numerically from the equation.
3. The two sets of data were compared with regard to the deviation at different segments of the data set.

The following list shows the maximum deviations found for the equations presented in the following paragraphs:

Two-dimensional model, semi-infinite conditions:
Equations 12, 13, 14, 16, 17: $< 1 \times 10^{-6}\%$
Equation 23: $< 0.05\%$
Three-dimensional model, semi-infinite conditions:
Equations 18, 25: $< 0.03\%$

Two-dimensional model

A feature of the semi-infinite diffusion conditions is the straight equiconcentration lines, the slope of which is a function of the ratio of the individual diffusion coefficients D_{C^+}, and D_{e^-}, respectively (Fig. 4). A corresponding chronoamperometric plot is shown in Fig. 5. The main feature is that the curve of the total current approaches a steady state value. The time dependence of the total current was found to follow Eq. 12:

$$I(t) = \frac{FY}{V_m} \left\{ \frac{1}{1 + \exp(-\varphi)} \right\} \times \left[\left(\frac{\Delta x_0 \sqrt{D_{e^-}} + \Delta z_0 \sqrt{D_{C^+}}}{2\sqrt{\pi t}} \right) + \sqrt{D_{e^-} D_{C^+}} \right] \tag{12}$$

A separation of the individual contributions of the bulk and surface boxes with the help of a separated analysis of the concentration changes of these boxes led to the conclusion that both the bulk current, $I_b(t)$, and surface current, $I_s(t)$, are time dependent:

$$I_s(t) = \frac{FY}{V_m} \left\{ \frac{1}{1 + \exp(-\varphi)} \right\} \left(\frac{\Delta x_0 \sqrt{D_{e^-}} + \Delta z_0 \sqrt{D_{C^+}}}{\sqrt{\pi t}} \right) \tag{13}$$

$$I_b(t) = \frac{FY}{V_m} \left\{ \frac{1}{1 + \exp(-\varphi)} \right\} \times \left[\sqrt{D_{e^-} D_{C^+}} - \left(\frac{\Delta x \sqrt{D_{e^-}} + \Delta z \sqrt{D_{C^+}}}{2\sqrt{\pi t}} \right) \right] \tag{14}$$

The effect of the increasing bulk current can be interpreted as a result of a growing of the reaction zone (see

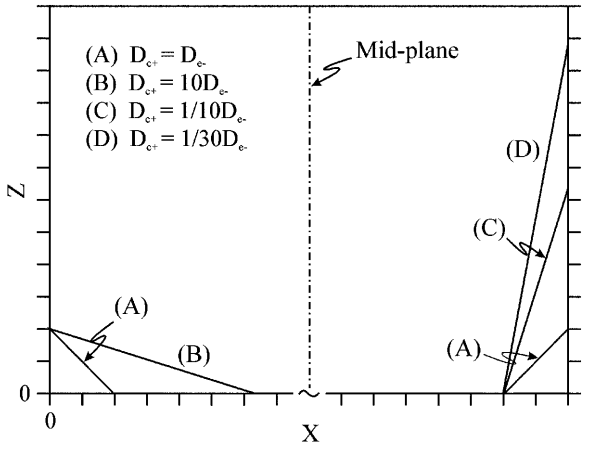

Fig. 4 Isoconcentration lines for different ratios of D_C^+/D_{e^-}, derived from two-dimensional, semi-infinite conditions

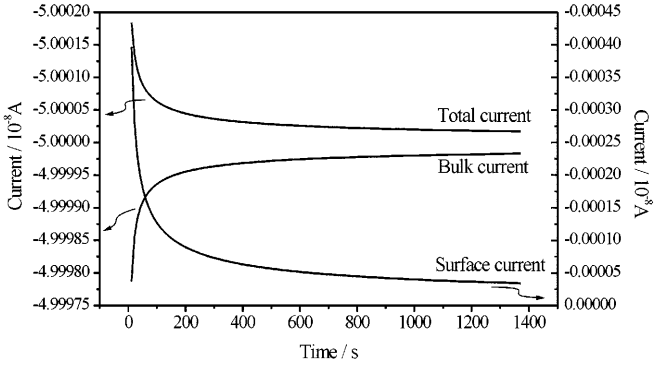

Fig. 5 Chronoamperogram for a potential step to a value 200 mV more negative than the formal potential: $D_{e^-} = D_{C^+} = 5 \times 10^{-8}$ cm^2 s^{-1}, $\Delta x_0 = \Delta z_0 = 10^{-4}$ Δx; the currents are normalized to the value of the diffusion coefficients

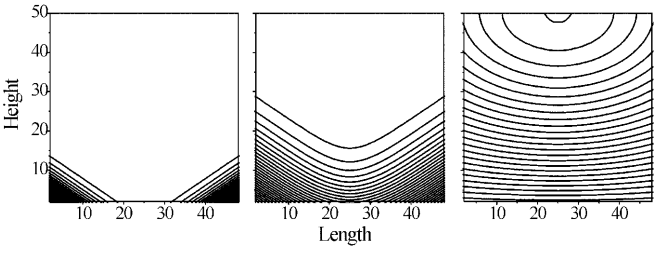

Fig. 6 Concentration profile of a partially converted two-dimensional model of a microcrystal at different times after a potential step of **A** 3 s, **B** 10 s, and **C** 40 s; $D_{e^-} = 5 \times 10^{-9}$ cm^2 s^{-1}, $D_{C^+} = 10^{-8}$ cm^2 s^{-1}

Fig. 6a). In most cases, the time dependencies can be neglected since the surface layers (Δx_0, Δz_0) are assumed to have atomic thickness. Thus the time-dependent term becomes small compared to the steady-state term. Equation 12 thereby can be simplified to:

$$I(t) = \frac{FY}{V_m}\left\{\frac{1}{1+\exp(-\varphi)}\right\}\sqrt{D_{e^-}D_{C^+}} \tag{15}$$

This simplification cannot be applied if one of the diffusion coefficients becomes zero. Then, the reaction remains surface confined and the steady-state term vanishes:

$$I_s(t) = \frac{FY\Delta x_0}{V_m}\left\{\frac{1}{1+\exp(-\varphi)}\right\}\sqrt{\frac{D_{e^-}}{\pi t}} \quad \text{for} \quad D_{C^+} = 0, \tag{16}$$

or

$$I_s(t) = \frac{FY\Delta z_0}{V_m}\left\{\frac{1}{1+\exp(-\varphi)}\right\}\sqrt{\frac{D_{C^+}}{\pi t}} \quad \text{for} \quad D_{e^-} = 0, \tag{17}$$

Three-dimensional model

The results of the two-dimensional model cannot simply be transferred to cuboid crystals, since the three-phase junction of these objects include the edges of the rectangular base, with the consequence that the cations enter the crystal from different directions.

In order to model the three-dimensional diffusion conditions the crystal|electrolyte interface plane (x,0,z) (Fig. 3a) was introduced. This allows taking into consideration the additional cation diffusion in the y-direction. This three-dimensional model should more realistically describe the diffusion processes inside a rectangular solid.

The first step was to model the semi-infinite diffusion conditions ($0 < x,y,z < \infty$). The current/time curve differs remarkably from the two-dimensional approach. The chronoamperograms were found to follow Eq. 18:

$$I(t) = \frac{F}{V_m}\left\{\frac{1}{1+\exp(-\varphi)}\right\} \times \left[Y\left(\left(\frac{\Delta x_0\sqrt{D_{e^-}} + \Delta z_0\sqrt{D_{C^+}}}{2\sqrt{\pi t}}\right) + \sqrt{D_{e^-}D_{C^+}}\right) - D_{C^+}\sqrt{2D_{e^-}t}\right] \tag{18}$$

Compared to the result of the two-dimensional model (Eq. 12), an additional subtractive term occurs. Interestingly, this term was found to be independent of the length of the three-phase junction. It has to be interpreted as an "edge effect" describing the overlapping of the cation diffusion (which now proceeds in x and y directions) near the corner and thereby its influence on the entire diffusion process.

Finite diffusion space

As was demonstrated in the above paragraphs, Eqs. 12 and 18 are the consequence of a diffusion of electrons and cations into a semi-infinite space. This diffusion,

which is accompanied by the growing of the reaction zone, is not necessarily confined to the condition of a really semi-infinite diffusion space, but can also be expected to apply to the beginning of the conversion of a crystal of limited size. Since crystals used for the voltammetry of microparticles have a very small size (1–100 μm) and experiments are usually performed within a time scale where total conversion of the material may take place, an unhindered diffusion can be assumed only for the initial period of the reaction. Now, the most important question will be: how do the diffusion barriers given with the crystal size and shape determine the advance of the electrochemical conversion through the crystal?

The large number of crystalline inorganic and organic compounds goes along with a great variety of crystal shapes, based upon different crystal structures and morphologies. It is obvious that even the restriction to rectangular crystals gives an infinite number of shapes based upon different ratios of crystal length, height and breadth. Additionally, one should keep in mind that a rectangular crystal with a certain geometry can be attached to an electrode surface by any of its three different faces. The combination of different crystal geometries and orientations with the individual diffusion coefficients of the cations (D_{C}^{+}) and electrons (D_{e^-}) produces a wealth of quite special conditions. It is not the aim of this paper to describe all these special conditions. It will be the aim to demonstrate how geometric and physical properties may govern the electrochemical conversion of a single rectangular microcrystal attached to an electrode surface.

In the following paragraphs the exhaustive electrochemical conversion of a microcrystal will be explained by help of two- and three-dimensional models (Fig. 3b). For the reason of clarity, most cases are described only by means of the dominant and most significant segments of the chronoampermometric curves.

The exhaustive conversion of the attached microcrystal will be described with the help of exponential functions of the general type $I = A\exp(-Bt)$. All functions are derived from the numerically simulated I vs. t data sets. The maximum deviation of the derived equations in relation to the simulated data was 0.5% for the pre-exponential factor (A) and 2% for the exponent, B.

Two-dimensional model – Finite diffusion space

During the modelled conversion the iso-concentration curves, which are straight lines at the beginning of the reaction, not only change their shape but also change their spreading direction (compare Fig. 6a–c). This process reflects the extent of the reaction and the ratio of individual diffusion coefficients as well as the geometry of the crystal. In order to take this point into consideration, the current-time functions will be described for different conditions.

To interpret the behavior at different time scales the terms "short time" and "long time" are used, which indicate the extent of the reaction. They are meant to be relative terms, depending on parameters like diffusion coefficients and grid size. The "short time" term indicates that only a little conversion has taken place, whereas "long time" corresponds to the majority of the material having been converted.

The short time behavior can be described with the results obtained for the semi-infinite condition (Eq. 12) and its simplified form (Eq. 15). The chronoamperograms are characterized by a time-independent steady-state current.

To describe the long time behavior, there are three conditions to be discussed. They depend on the ratio of the diffusion coefficients D_{e^-} and D_{C}^{+} in relation to the dimensions of the grid:

$$v_{C^+} = \frac{4D_{C^+}}{L^2} \text{ and } v_{e^-} = \frac{D_{e^-}}{H^2} \tag{19}$$

where the factor 4 comes from the symmetry of the model, which has the consequence that only $L/2$ has to be taken into the calculation. The v-values give a measure for how fast an electron or cation can pass a certain distance (given the particle dimensions).

$v_{C^+} = v_{e^-}$. The most characteristic segment is the very end of the conversion (where 99–99.999% of the compound is already reduced). This segment has been analyzed with the help of exponential fitting methods and the following dependence was found:

$$I(t) = \frac{8FYD_{e^-}D_{C^+}t}{V_m HL}\left\{\frac{1}{1+\exp(-\varphi)}\right\}\exp\left[\frac{-\pi^2 v_{\pm}t}{4}\right] \tag{20}$$

where $v_{\pm} = \frac{D_{e^-}}{H^2} = \frac{4D_{C^+}}{L^2}$.

$v_{C^+} > v_{e^-}$. Owing to a relatively fast cation diffusion, the reaction zone spreads along the crystal|electrode interface much faster than in the z-direction (for illustration, see Fig. 4, equiconcentration line B). It reaches the midplane of the crystal ($L/2$,z), where both diffusion routes, (1) coming from $x = 0$ and (2) coming from $x = L$, meet. Both reaction zones fuse, as seen in Fig. 6, leading to a bowl-shaped "filling up" of the reduced species parallel to the electrode surface. The exhaustive reaction along the x-direction has the consequence that this diffusion vector will be lost and instead the diffusion in the z-direction determines the further conversion. Depending on the ratio $v_{C^+} > v_{e^-}$, the overall current-time function will be dominated by this process. Thus, the ratio $v_{C^+} > v_{e^-}$ with a magnitude greater than 10^3 was found to cause a nearly pure planar diffusion process typical for single-working-electrode thin layer cells [8]

$$I(t) = \frac{2FYLD_{e^-}}{V_m H}\left\{\frac{1}{1+\exp(-\varphi)}\right\}\sum_{j=1}^{\infty}\exp\left[\frac{-(2j-1)^2\pi^2 D_{e^-}t}{4H^2}\right] \tag{21}$$

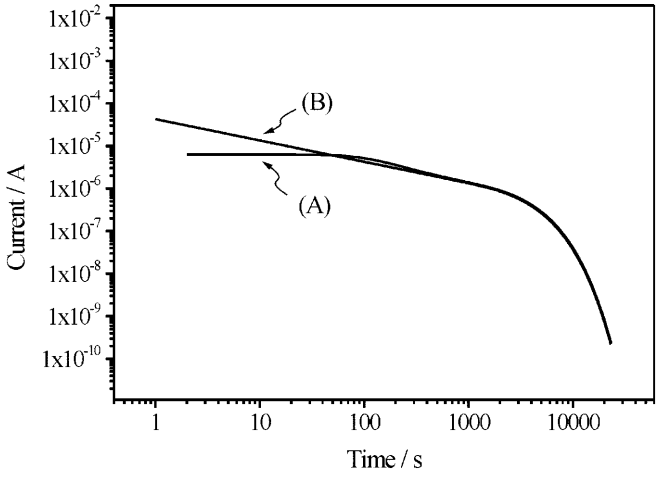

Fig. 7 Comparison of a simulated potential-step experiment and the derived current/time dependence (Eq. 21); two-dimensional model with $L = 25$ μm, $H = 25$ μm, $y = 1$ cm, $D_{C^+} = 10^{-8}$ cm^2 s^{-1}, $D_{e^-} = 10^{-9}$ cm^2 s^{-1}, $V_m = 153.8$ cm^3 mol^{-1}

Strictly speaking, Eq. 21 is of course a limiting case, which is based upon cations being freely mobile in the bulk of the crystal. In this case, the conversion depends only on the diffusion of electrons from the electrode into the bulk.

The smaller the ratio $v_{C^+} > v_{e^-}$ becomes, the more stress must be laid on the cation diffusion and the more the graph of Eq. 21 differs from the chronoamperogram obtained with help of the numerical simulation. Interestingly, this divergence applies only to the initial time of the conversion, at which Eq. 12 is valid. With the advancing reaction, the graph of Eq. 21 approaches the simulated curve (see Fig. 7). The smaller the ratio $v_{C^+} > v_{e^-}$ becomes, the later both curves approach.

$v_{C^+} < v_{e^-}$. The opposite situation occurs with a ratio v_{C^+}/v_{e^-} smaller than 10^{-3}. The reaction progress is governed by the slower cation diffusion in the x-direction. The simulated chronoamperometric plots are dominated by a diffusion process typical of a twin-electrode thin layer cell [8]:

$$I(t) = \frac{FYHD_{e^-}}{V_m L}\left\{\frac{1}{1+\exp(-\varphi)}\right\}\sum_{j=1}^{\infty}\exp\left[\frac{-(2j-1)^2\pi^2 D_{e^-}t}{L^2}\right] \tag{22}$$

The larger v_{e^-} becomes, compared to v_{C^+}, the more the electron diffusion along the top face of the crystal has to be taken into consideration. Finally, the three-phase junction reaction can be replaced by a two-phase reaction (solid/electrolyte). Figure 8 clarifies this situation: the electrons "creep " along the crystal/electrolyte surface layer, which is converted immediately. The cation diffusion into the crystal is rate determining. Equation 23 describes the initial period of the reaction of an electronically conductive solid compound. Here, the electrode potential applies to the whole surface of the crystal and the bulk reaction is a function of the cation diffusion only:

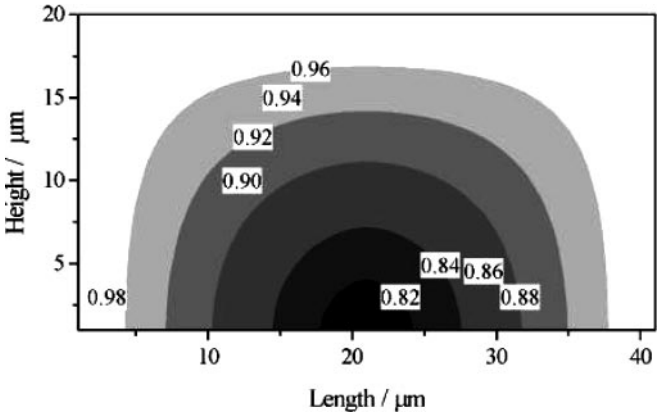

Fig. 8 Cross-section of the concentration profile of a partially converted microcrystal in the x-z plane for $y = 20$ μm and a square base of 40 μm; $D_{e^-} = 5000\ D_{C^+}$

$$I(t) = \frac{FY}{V_m}\left\{\frac{1}{1+\exp(-\varphi)}\right\}\left[\frac{(2H+L)\sqrt{D_{C^+}}}{\sqrt{\pi t}} - 2.5D_{C^+}\right] \tag{23}$$

The further course of the reaction is determined by the shape (ratio of length, height and breadth) of the crystal: the reaction is dominated by diffusion through the larger crystal|solution interface (top face or side face). Thus, typical single-working-electrode thin film behavior can be observed for $H \ll L$ (flat crystals). Here, the simulated chronoamperometric curves follow Eq. 24:

$$I(t) = \frac{2FAD_{e^-}}{V_m H}\left\{\frac{1}{1+\exp(-\varphi)}\right\}\exp\left[\frac{-\pi^2 D_{e^-}t}{4H^2}\right] \tag{24}$$

Equation 24 includes only the first term of an exponential series and describes the very end of the conversion (> 99.5%) only.

For a reaction which is based upon the assumed independent (but coupled!) diffusion of electrons and cations, the following conclusions can be made: even though the initial conversion steps are confined to the three-phase junction, i.e. the electrode|electrolyte|crystal boundary, the reaction transforms into a typical two-phase reaction based upon the slowest diffusion process, either the cation diffusion through the crystal|solution interface or the electron diffusion through the crystal|electrode interface.

Three-dimensional model; finite diffusion space

For a certain geometry (may be a cube or a cuboid) of the microcrystal, the ratio D_{e^-}/D_{C^+} determines the spatial course of the reaction zone and thereby the resulting current/time function. Figure 9 shows the isoconcentration lines along the (x,y) plane at half height for two differently shaped cuboids after a partial reduction of the particle. Here, the problem of deriving a "general equation" for the current/time function becomes obvious. The progress of the reaction zone follows different

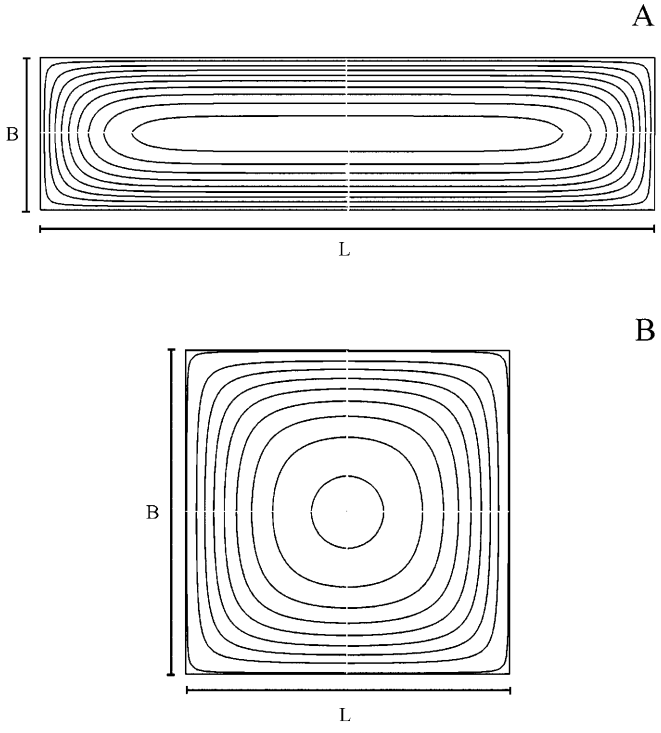

Fig. 9A,B Concentration profile inside partially (10%) converted crystals; cross section through the *x-y* plane at half height; **A** crystal of $L = H = 10$ μm, $B = 40$ μm and **B** $L = B = H = 10$ μm size

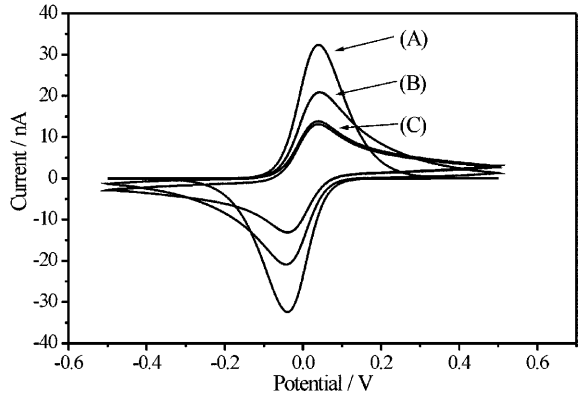

Fig. 10 Cyclic voltammograms of differently shaped cuboid particles of constant volume with a square base of different size; $D_{e^-} = D_{C^+} = 10^{-8}$ cm^2 s^{-1}, $V_m = 153.8$ cm^3 mol^{-1}, (*A*) $L = B = 28$ μm, $H = 10$ μm, (*B*) $L = B = H = 20$ μm, (*C*) $L = B = 16$ μm, $H = 31$ μm

reaction geometries, causing tremendous changes in the chronoamperometric curve. This can also be observed from the different shapes of the cyclic voltammograms demonstrated in Fig. 10. The voltammograms are the result of a simulated cyclic oxidation and reduction of differently shaped cuboids of a uniform volume. Depending on the ratio of crystal height, length and breadth, different diffusion regimes dominate the reaction and determine the time for the total conversion of the solid. These diffusion regimes are similar to the

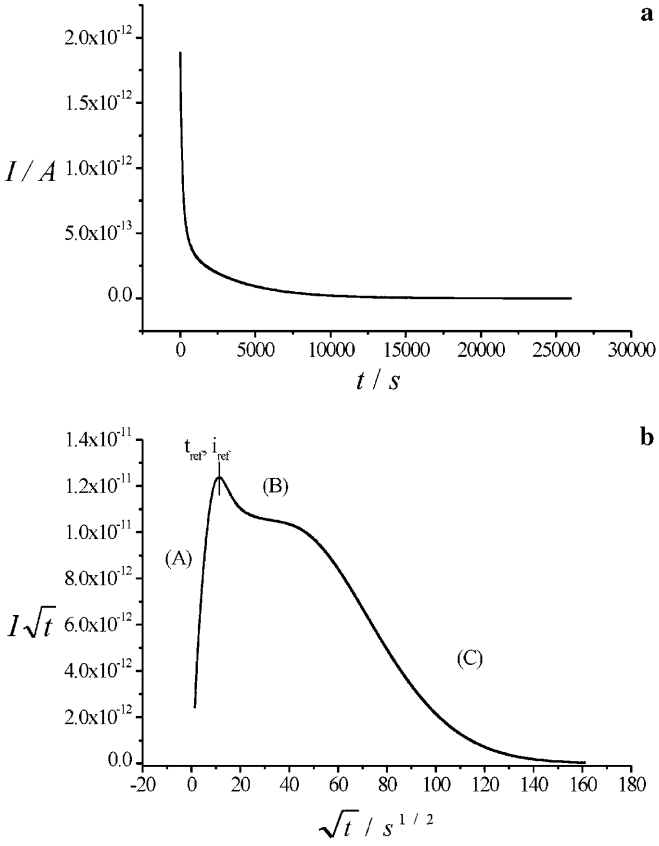

Fig. 11a,b Chronoamperogram of the electrolysis of a microcrystal ($20 \times 20 \times 20$ μm), $D_{e^-} = D_{C^+} = 10^{-8}$ cm^2 s^{-1}, $V_m = 153.8$ cm^3 mol^{-1}; **a** I vs. t plot; **b** $I\sqrt{t}$ vs. $\sqrt{t}$ plot

process of the conduction of heat in rectangular parallelepipeds [9].

To interpret the chronoamperometric plots it is helpful to split the $I(t)$ curves into distinct time stages, which represent the extents of the conversion, and which are defined by different functions. Figure 11 shows the chronoamperometric plot of the electrolysis of a cuboid microparticle as the usual current vs. time plot (Fig. 11a) and as $I\sqrt{t}$ vs. $\sqrt{t}$ (Fig. 11b). Clearly, different stages (in the following paragraphs marked with A and B and C) can be distinguished. The stages have been analyzed and the current/time equations have been derived from the curve fitting results.

Stage A. Stage A ("short time") denotes the initial period of the reaction. During this period, quasi semi-infinite conditions apply to the diffusion of both electrons and cations. As expected, the resulting current/time functions are based upon Eq. 8:

$$I(t) = \frac{F}{V_m}\left\{\frac{1}{1+\exp(-\varphi)}\right\}\left[u\left(\left(\frac{\Delta x_0\sqrt{D_{e^-}} + \Delta z_0\sqrt{D_{C^+}}}{2\sqrt{\pi t}}\right) + \sqrt{D_{e^-}D_{C^+}}\right) - 4D_{C^+}\sqrt{2D_{e^-}t}\right] \quad (25)$$

Here, u is the length of the three-phase junction (perimeter of the electrode|crystal interface). The "edge

term'' of Eq. 18 had to be multiplied by the number of edges of the rectangular base to form Eq. 25.

Stage B. Mainly, there are two conditions to be discussed. Analogously to the two-dimensional model, they depend on the ratio of the diffusion coefficients D_{e^-} and D_{C^+} related to the dimensions. Owing to the fact that the cations enter the crystal through two interfaces whereas the electrons enter through one interface only, v_{C^+} (Eq. 19) has to be replaced by the modified quantity $v^*_{C^+}$:

$$v^*_{C^+} = f_{\text{shape}} \frac{4D_{C^+}}{L^2} \text{ with } 0.5 < f_{\text{shape}} < 1 \tag{26}$$

where f_{shape} represents a dimensionless factor, arising from the overlapping of the cation diffusion in the x-direction and the y-direction and thus from the ratio of the crystal length (L) and crystal width (B). It was determined from simulation results to reach 1 for $L \gg B$ and 0.5 for $L = B$.

$v^*_{C^+} > v_{e^-}$ The diffusion of the cations is fast compared to the diffusion of the electrons. This means that during the initial period (Fig. 11, stage A) the cations spread along the electrode|crystal interface into the bulk. Very quickly, the oxidized centers along this interface are exhausted, with the consequence that Eq. 25, which is based upon the unhindered diffusion of both cations and electrons, loses its validity. Now, the electron diffusion (in the z-direction) becomes rate determining. This means that after an initial period in which Eq. 25 is valid, the orientation of the equiconcentration lines becomes more and more parallel to the electrode surface.

The maximum value t_{ref} of the $I\sqrt{t}$ vs. $\sqrt{t}$ plots (Fig. 11) was found to be a characteristic time to describe the point at which the transition from the three-dimensional diffusion conditions (Eq. 25) to the planar (two-dimensional) diffusion occurs. The value of t_{ref} was found to follow Eq. 27. The accompanying current value at t_{ref} corresponds to Eq. 28.

$$t_{\text{ref}} = \frac{L^2 B^2}{4.45(L^2 + B^2) D_{C^+}} \tag{27}$$

$$I_{\text{ref}} = 0.75 \frac{Fu}{V_m} \sqrt{D_{e^-} D_{C^+}} \left[1 - \frac{LB}{(L+B)\sqrt{1.1(L^2+B^2)}} \right] \tag{28}$$

It could be feasible to use these values (derived from a single-crystal potential step experiment) for the determination of the individual diffusion coefficients or to determine the geometric parameters of the studied crystals.

Analogously to the two-dimensional model (cf. Fig. 7), the chronoamperograms approach a dependence, characteristic for planar diffusion conditions, and which can be described by Eq. 29:

$$I(t) = \frac{2FAD_{e^-}}{V_m H} \left\{ \frac{1}{1+\exp(-\varphi)} \right\} \sum_{j=1}^{\infty} \exp\left[\frac{-(2j-1)^2 \pi^2 D_{e^-} t}{4H^2} \right] \tag{29}$$

The larger is the ratio v_{C^+}/v_{e^-} is the more rate determining the electron diffusion becomes and the faster both curves merge. For ratios $v^*_{C^+}/v_{e^-} < 10$ this happens only at the very end of the conversion. Nevertheless, this final reaction state (ratio of converted crystal >99%) can be described by the first term ($j = 1$) of Eq. 29:

$$I(t) = \frac{2FAD_{e^-}}{V_m H} \left\{ \frac{1}{1+\exp(-\varphi)} \right\} \exp\left[\frac{-\pi^2 D_{e^-} t}{4H^2} \right] \tag{30}$$

$v^*_{C^+} < v_{e^-}$. During the initial reaction period (section A in Fig. 11) the reaction zone spreads in the z-direction and reaches the top surface of the crystal. The redox centers in the vicinity of the crystal|electrolyte interface are converted quickly. The cation diffusion into the bulk, in the x and y directions, now becomes rate determining.

The end of section A, t_{ref}, was determined to follow Eq. 31:

$$t_{\text{ref}} = \frac{H^2}{1.1 \cdot D_{e^-}} \tag{31}$$

At this time, the current was found to be:

$$I_{\text{ref}} = 0.72 \frac{Fu}{V_m} \sqrt{D_{e^-} D_{C^+}} \tag{32}$$

The crystal will now be converted, advancing from the crystal|solution interface into the bulk. The most characteristic part is the end of the conversion (see Fig. 11b, section C). Here, the chronoamperometric curves can be characterized by Eq. 34 or Eq. 35, depending on the narrowest breadth B of the cuboid.

For solids with a square base ($B = L$):

$$I(t) = 3.3 \frac{FHD_{C^+}}{V_m} \left\{ \frac{1}{1+\exp(-\varphi)} \right\} \exp\left[\frac{-2\pi^2 D_{C^+} t}{L^2} \right] \tag{34}$$

For $B \ll L$:

$$I(t) = \frac{FLHD_{C^+}}{V_m B} \left\{ \frac{1}{1+\exp(-\varphi)} \right\} \exp\left[\frac{-\pi^2 D_{C^+} t}{B^2} \right] \tag{35}$$

At the first glance it seems surprising that Eq. 34 is not to equal Eq. 35. The result becomes clearer taking Fig. 9 into consideration: in the case of $L = B$, all the four crystal|solution interfaces equally contribute to the exhaustive conversion. For $L > B$, the diffusion conditions become similar to a twin-electrode thin film cell.

Conclusions

The electrochemical reduction of a microcrystal attached to an electrode has been described theoretically by the help of two- and three-dimensional models. Depending on the crystal geometry, the simulated voltammetric behavior for the three-dimensional model differs remarkably from the two-dimensional model.

The geometry of the spatial development of the reaction zone as a function of the diffusion coefficients, of the crystal size and crystal shape determines the

mathematical functions and therefore the shape of the chronoamperograms.

An important result of this study is the observation that in the case of different individual diffusion coefficients of the cations and electrons – which is a reasonable assumption for real systems – the reaction at the three-phase junction only initially determines the course of the reaction. During this initial three-phase reaction, the faster process leads to an exhaustive conversion along the corresponding interface either the crystal|electrode interface, or the crystal|solution interface. The further course of the conversion into the crystal bulk is determined by the slowest diffusion process. This process involves only two phases: (1) electrode/crystal in case of slow electron diffusion, or (2) solution/crystal in case of a slow cation diffusion. This transition to the two-phase condition is the reason that a number of equations of the exhaustive conversion are similar to those known, for example, for planar diffusion conditions.

The results of this study can, in principle, be utilized to determine the diffusion coefficients from experimental data and also to derive the geometric parameters of the attached crystals. However, in real experiments with immobilized microcrystals this will be difficult, as usually an assembly of different crystals with a certain shape and size distribution will be immobilized on the electrode surface. Hence it will be necessary to focus future work on the behavior of microcrystal arrays with a known shape and size distribution. Another factor which has to be taken into account is the slow kinetics of electron transfer at the electrode|solid interface.

The model of an independent and perpendicular diffusion of cations and electrons – which was the basis for the simulation – is an assumption, which has to be corroborated by future experimental work. It is essential to combine theoretical and experimental efforts to illuminate the mechanisms of the insertion solid state electrochemical reactions.

Acknowledgements U.S. would like to thank the Hans Böckler Foundation for financial support. K.B.O., J.C.M. and P.J.M. thank the Natural Sciences and Engineering Research Council of Canada.

References

1. Lovric M, Scholz F (1997) J Solid State Electrochem 1: 108–113
2. Scholz F, Meyer B (1998) Voltammetry of solid microparticles immobilized on electrode surfaces. In: Bard A, Rubinstein I (eds) Electroanalytical Chemistry, vol 20. Dekker, New York, pp 1–86
3. Weppner W (1995) Electrode performance. In: Bruce PG (ed) Solid state electrochemistry. Cambridge University Press, Cambridge, pp 199–228
4. Oldham KB (1998) J Solid State Electrochem 2: 367–377
5. Feldberg SW (1981) J Electroanal Chem 127: 1
6. Jaworski A, Stojek Z, Scholz F (1993) J Electroanal Chem 354: 1
7. Weppner W (1997) Principles of main experimental methods. In: Gellins PJ, Bouwmeester HJM (eds) The CRC handbook of solid state electrochemistry. CRC Press, Boca Raton, pp 296–299
8. Bard AJ, Faulkner LR (1980) Electrochemical methods. Wiley, New York, pp 406–413
9. Carslaw HS, Jaeger JC (1959) Conduction of heat in solids, 2nd edn. Clarendon Press, Oxford, pp 176–185